ADVANCED THEORY AND SIMULATIONS
www.advtheorysimul.com

Effect of Anion Hydrophobicity on the Oxidation of Ferrocene-Terminated Monolayers

*Ludwig J.V. Ahrens-Iwers, Gregor B. Vonbun-Feldbauer, and Robert H. Meißner**

Self-assembled monolayers (SAMs) terminated with ferrocene (Fc) moieties are a popular model system for electron transfer processes at solid-liquid interfaces. Numerous experimental studies have found a correlation between the hydrophobicity of anions in the electrolyte and the redox potential. In this computational study, the redox potential is calculated for various anion species and SAM configurations using classical molecular dynamics. Thermodynamic integration and the constrained charge method are used to determine the redox potential as the free energy change associated with electron transfers from the Fc moieties to the electrodes. The results show the anticipated lower redox potentials for hydrophobic anions and allow the study of changes at the solid-liquid interface at the atomistic level.

1. Introduction

Electrodes can be functionalized by molecules at solid–liquid interfaces, leading to complex electrochemical properties with potential applications in energy harvesting devices,[1] sensors and actuators.[2,3] Ferrocenylalkanethiolates (SC_nFc) can be used to build Fc-terminated self-assembled monolayers (SAMs) on gold electrodes as shown in **Figure 1**. These SAMs provide model systems for the study of electron transfers at interfaces and have been the subject of numerous experimental studies.[4–12] The properties of the SAM and the electrochemical environment can be precisely controlled allowing for investigations of their effects on the electron transfer. For instance, the surface concentration of Fc,[9] the choice of the Fc derivative[13] and the length of carbon chains[5,6] have been shown to affect the electrochemical properties.

L. J. Ahrens-Iwers, G. B. Vonbun-Feldbauer, R. H. Meißner
Institute for Interface Physics and Engineering
Hamburg University of Technology
21073 Hamburg, Germany
E-mail: robert.meissner@tuhh.de

R. H. Meißner
Institute of Surface Science
Helmholtz-Zentrum Hereon
21502 Schleswig-Holstein, Germany

The ORCID identification number(s) for the author(s) of this article can be found under https://doi.org/10.1002/adts.202500860

DOI: 10.1002/adts.202500860

Several computational studies of Fc-terminated SAMs have modeled the free energy of the electron transfer between the Fc moiety and the working electrode, i.e., the redox potential in the experiment. These studies have focused on either the electronic structure[15,16] or the dynamics.[17–19] Notably, studies on the redox potential calculate the difference in free energy between the two states at equilibrium. This is in contrast to the reorganization energy in Marcus theory,[20] which is related to an electrolyte reorganization without a change in the electronic state. Further, calculations of the redox potential do not necessarily make predictions regarding the rate of the electron transfer, as opposed to the Marcus theory. One contribution to the free energy of the redox reaction is the ionization energy of the Fc moiety, necessitating electronic structure calculations. Another contribution to the redox potential stems from changes in the electrolyte dynamics near the monolayer. The free energy of the electrolyte is determined by sampling over its thermodynamic ensemble. For Fc in bulk solution, a hybrid approach of quantum and classical methods along with a free energy perturbation (FEP) approach,[21] has included both effects and provided accurate redox free energies.[22] Unfortunately, a hybrid approach would be rather challenging for the more complex Fc-terminated SAMs. Nevertheless, studies focusing on individual aspects of the electron transfer have provided valuable insights into the process at the atomistic scale. On the one hand, a clear relationship between ionization energies and redox potentials[13] has been established and thus single-point electronic structure calculations can provide insight into the electron transfer. Density functional theory (DFT) calculations by Lima *et al.*[15] have shown that the electrolyte does not have a strong impact on the electronic structure, whereas other calculations[16] have shown an influence of coadsorbed species, i.e., other molecules within the SAM, on the ionization energy. On the other hand, classical molecular dynamics (MD) has been employed to model the electrolyte dynamics which contribute to the free energy change of the redox reaction. In particular, the effect of chain length[17,18] and monolayer composition in combination with different anion species[19] has been investigated using thermodynamic integration (TI).[23] In these studies, contributions to the free energy are calculated, which are not accessible via single-point DFT calculations. Especially for the large configuration space of the monolayer, classical MD has some advantages over ab-initio MD, since long trajectories of thousands of atoms may be required to adequately sample the phase space.

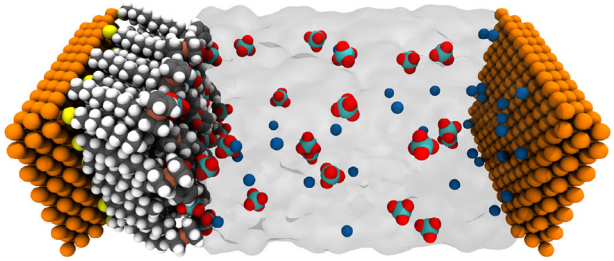

Figure 1. Model system of Fc-terminated monolayer on gold on the left covered by an aqueous solution which is confined by a computational counter electrode on the right. This image was rendered with VMD.[14]

In this study, Fc-terminated monolayers are modeled in classical MD. The free energy change due to oxidation is determined with TI together with the constrained charge method (CCM). Model systems with five different anions, $TFSI^-$, PF_6^-, ClO_4^-, BF_4^-, and NO_3^-, are analyzed. The use of different anions allows the effect of their hydrophobicity on the redox potential and structural changes at the solid–liquid interface to be studied at the atomistic scale.

2. Theoretical Methods

In this work, TI[23,24] is employed, which has also been used in refs. [17–19], to determine the difference in free energy between the cathodic system with neutral Fc moieties and the anodic system with oxidized ferrocenium (Fc^+) moieties. In contrast to previous work, the TI is combined with the CCM to transfer excess charges to the electrodes.

The TI yields the difference in free energy between two states of a system by slowly changing from one to the other. In our case, the two states are the cathodic and anodic states before and after oxidation. The two states differ by the atomic charges $q_i^{(\alpha)}$ within the Fc moiety, where i is the index of the respective atom and $\alpha \in \{0, 1\}$ denotes the cathodic and anodic state. In the TI, the atomic charges

$$q_i(\lambda) = (1-\lambda)q_i^{(0)} + \lambda q_i^{(1)} \tag{1}$$

are adiabatically switched by incrementally increasing the parameter λ from 0 to 1. The potential energy $U_\lambda(r)$ and thus the Hamiltonian $\mathcal{H}_\lambda(r,p)$ depend on this parameter. A shorthand notation is employed, wherein r and p represent the collective positions and momenta of all N atoms. Accordingly, we write the Helmholtz free energy

$$A(\lambda) = -\beta^{-1} \ln Q(\lambda) \tag{2}$$

with the partition function

$$Q(\lambda) = \frac{1}{N! h^{3N}} \int \mathrm{d}^{3N} r \int \mathrm{d}^{3N} p \exp\left[-\beta \mathcal{H}_\lambda(r,p)\right] \tag{3}$$

as a function of λ. Here, h is the Planck constant and $\beta = \left(k_\mathrm{B} T\right)^{-1}$ with the Boltzmann constant k_B and temperature T. A shorthand notation is used for the integration over the entire phase space of N atoms. We can now express the difference in free energy

$$\begin{aligned}\Delta A_{0\to1} &= \int_0^1 \mathrm{d}\lambda \frac{\partial A(\lambda)}{\partial \lambda} \\ &\approx \sum_k w_k \frac{A(\lambda_k + \delta\lambda) - A(\lambda_k)}{\delta\lambda}\end{aligned} \tag{4}$$

as an integral over λ which is computed numerically with weights w_k and a differentiation at λ_k with the finite difference $\delta\lambda$ in the finite difference TI.[24] The numerator

$$A(\lambda_k + \delta\lambda) - A(\lambda_k) = -\beta^{-1} \ln \left\langle \exp\left(-\beta\left[U_{\lambda_k+\delta\lambda}(r) - U_{\lambda_k}(r)\right]\right)\right\rangle_{\lambda_k} \tag{5}$$

can be determined by sampling over a finite difference in the potential energy at the respective value of λ_k. The difference in free energy in the reverse direction $\Delta A_{1\to0}$ can be defined analogously with an opposite sign and converges to the same value. The redox potential, $E^0_{0\to1} = \Delta A_{0\to1}/(eN_\mathrm{Fc})$, is the free energy change per transferred charge, where N_Fc is the number of Fc moieties.

The additional positive charge resulting from the transition from Fc to Fc^+ must be compensated in order to maintain charge neutrality. One option is to remove a cation from the aqueous solution at a rate equivalent to that of Fc oxidation.[17] In this study, we present a novel approach in which a negative charge is transferred to the electrodes. In order to distribute this charge across the electrodes, the CCM,[25] a variant of the constant potential method,[26,27] is employed for this. In the CCM method, the potential energy as a function of the atomic electrode charges is minimized with a constraint on the total electrode charge.

3. Computational Model

The model system is illustrated in Figure 1 and comprises a working electrode covered by a monolayer, which is covered by an aqueous electrolyte which is confined by a counter electrode. The two electrodes are composed of three layers of gold atoms in a fcc (111) oriented lattice. The electrolyte comprises Na^+ ions and an equal number of anions of one of the five species at a concentration of approximately 1 M in water.

In contrast to the experimental setup, the CCM does not apply a potential difference between the electrodes. The counter electrode in the experiment sets a potential difference, driving the oxidation. There is no direct equivalent for this in the model and instead, the oxidation is driven by the TI. The computational electrode is required to confine the electrolyte and accept excess negative charges. One could set a potential difference to model an electric field, but here we approximate the field as zero.

The thiolates are arranged in a $\sqrt{3}\times\sqrt{3}$ R30° layer on the (111) gold surface[4,28] generating a coverage of 1/3. In the setup depicted in **Figure 2**, thiolates are placed on top of gold atoms but during the subsequent relaxation they are moving to hollow sites. The adsorption to hollow sites is consistent with ab-initio results.[15] A fraction χ_Fc of the thiolates is terminated with Fc group ($Fe(C_5H_5)_2$). Two monolayers are generated with $\chi_\mathrm{Fc} = 1/4$ and $\chi_\mathrm{Fc} = 1/3$, and resulting surface concentrations of 1.9×10^{-10} and 2.6×10^{-10} mol cm^{-2}, respectively. The surface concentrations are about half as large as commonly found for full

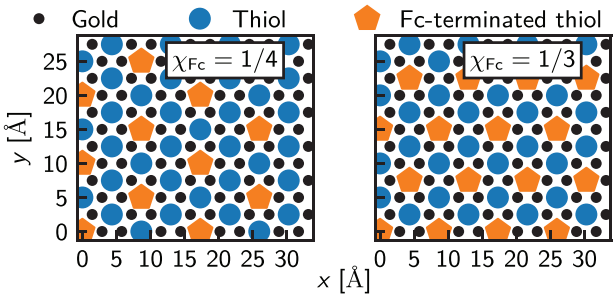

Figure 2. Top view of the monolayer configuration for two ferrocene SAMs, denoted by the fraction χ_{Fc}.

surface concentrations in experiments.[10,12] For high concentrations, buried Fc moieties have been observed[29] and we also encountered this in attempts to build such systems. Further, the coverage of the SAM may be decreased due to the large size of the Fc moieties. The models in this study are limited to small concentrations to avoid buried Fc moieties with low mobility which would complicate sampling over the thermodynamic ensemble in the TI. In our model system, the carbon chain in ferrocenylalkanethiolates has a length of 11 while the length is 10 in thiolates without Fc moiety. This choice is motivated by some of the experimental studies with mixed monolayers.[4,11] In studies with monolayers purely composed of ferrocenylalkanethiolates a chain length of 11 is also common.[8,10,12,30]

The TI yields the free energy change between the cathodic and anodic state. However, this does not include the ionization potential of the Fc moiety and the work function of the electrodes. These contributions include quantum effects[13] and cannot be adequately modeled in classical MD. However, they are not strongly dependent on the electrolyte.[15] Therefore, the differences between model systems with different anions are assumed to be negligible. Moreover, our models include the changes in free energy at the counter electrode, i.e., only setups with the same fraction χ_{Fc} can be compared, as the changes at the counter electrode are nearly identical in this case.

4. Computational Details

The parameters for the chain and headgroup of thiolates were taken from the OPLS-AA[31] force field with simplified charges from ref. [32]. The force field for metallocenes, as proposed by ref. [33], was utilized for Fc, and the charges of Fc^+ were obtained from ref. [17]. The gold parameters were taken from ref. [34] and the reciprocal width of electrode atoms was 1.979Å^{-1}.[27] The force field setup for the monolayer was based on the work of Malfreyt and coworkers.[17,19,35,36] The OPLS-2009IL[37,38] parameters were used for all of the anions and Na^+ parameters are taken from OPLS-AA.[31] Water was modeled with the TIP3P water model.[39] Geometric mixing was used to obtain Lennard–Jones parameters for interactions between atoms of different species.

All MD simulations were performed with the Large-scale Atomic/Molecular Massively Parallel Simulator (LAMMPS).[40] The CCM implementation in the ELECTRODE package[25] was used to distribute charges within the electrodes. The TI was conducted using the FEP package which was modified to ensure compatibility with the ELECTRODE package by updating electrode charges for perturbations.[41] The 3D Ewald summation with dipole correction[42,43] was used to compute Coulomb interactions for a system with one non-periodic direction. The particle-particle particle-mesh algorithm was employed to accelerate calculations.[44] All calculations used an NVT ensemble at 300 K with a Nosé–Hoover thermostat.[45,46] The system was equilibrated with the top electrode at atmospheric pressure using the conjugate gradient algorithm in the CCM to allow for a moving electrode. An exemplarily input script to achieve this is available as an example in the ELECTRODE package. Subsequent trajectories to sample for the TI were obtained with fixed electrodes using matrix inversion method. Systems were generated using Moltemplate.[47]

Table 1. Redox potential for different anion species at fractions 1/4 and 1/3, and the free energy of hydration for the respective anion. The redox potential E^0 is the arithmetic mean of redox potentials $E^0_{0\to1}$ and $E^0_{1\to0}$, calculated from forward and backward TI, respectively. The free energy of hydration is calculated via TI of individual ions in bulk water with an NPT ensemble.

Anion	$E^0_{1/4}$ [V]	$E^0_{1/3}$ [V]	ΔA_{hyd} [eV]
$TFSI^-$	1.25	1.73	−0.4
PF_6^-	1.32	1.74	−3.1
ClO_4^-	1.35	1.74	−3.4
BF_4^-	1.38	1.79	−3.5
NO_3^-	1.40	1.82	−4.0

5. Results

The computed redox potentials E^0 at the two fractions and the hydration energies for the five anions are presented in **Table 1**. The absolute values of E^0 have an unknown offset, i.e., only values within one column can be compared. The five anions are listed in ascending order of their redox potentials in experiments.[7,8,10–12,30] All values are in the expected order except for a small deviation for $E^0_{1/3}$ of PF_6^-. The differences in E_0 between anion species are in a reasonable range compared to experiment. The hydration energy of $TFSI^-$ is in the expected order but notably smaller than for the other anions.

Figure 3 shows the number density profiles of anions over the distance to the gold surface for the two fractions and the five anions. In the cathodic state in the left panels, $TFSI^-$ builds a layer with two peaks near the Fc moieties, which are at a distance of about 17.3 Å to the gold surface whereas all other anion species do not form layers. In the anodic state, an increase of the number densities near the Fc^+ cations is observed for all anion species. The layers are most pronounced for $TFSI^-$ and PF_6^-, and less pronounced for more hydrophilic anions, especially NO_3^-. All anion species show peaks near the Fc^+ cations with peak height in the same order as their redox potentials and hydration energies in Table 1.

Experimental studies have used Raman spectroscopy[7] and X-ray photoelectron spectroscopy[12] to detect anion layers at Fc-terminated SAMs. For all anion species in this work, anion layers have been detected in the anodic but not in the cathodic state. The absence of a $TFSI^-$ layer in the cathodic state has been proved experimentally,[12] i.e., the computational results for this anion

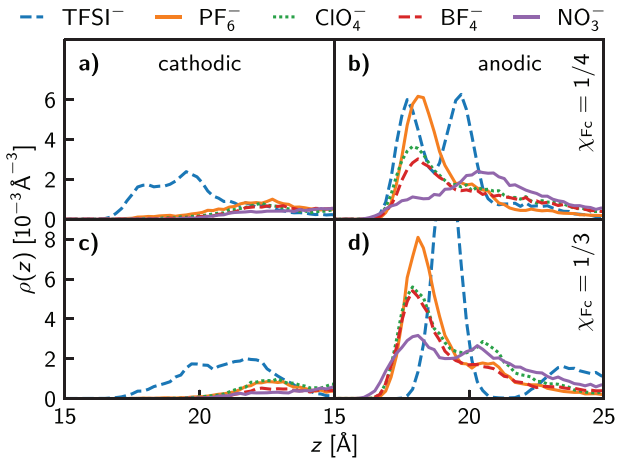

Figure 3. Number densities of anions as a function of distance to the gold surface in the cathodic (a, c) and anodic (b, d) state for fractions 1/4 (a, b) and 1/3 (c, d).

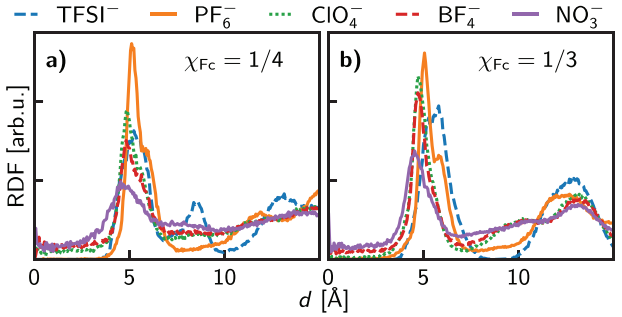

Figure 4. RDFs of anion-Fc distances in the *xy*-plane in the anodic state.

are unreliable. Presumably, the hydrophobicity is overestimated in the OPLS-2009IL force field which would explain the low hydration energy and the layering in the cathodic state. The four other anions, PF_6^-, ClO_4^-, BF_4^- and NO_3^-, are in the expected order in both redox potential and hydration energy. Experimental studies have found a less pronounced layering[7] and hindered oxidation[10] for NO_3^- compared to PF_6^-, ClO_4^- and BF_4^-. This is consistent with the density profiles in Figure 3 and larger redox potential for NO_3^-, while the profiles of PF_6^-, ClO_4^- and BF_4^- are similar but still a trend for larger peaks for the more hydrophobic anions is observed.

The anion structure at the interface is further analyzed using radial distribution functions (RDFs) of the anion-Fc distances in the *xy*-plane, as shown in **Figure 4**. The distances are calculated between the center atom of each anion and the iron atom in the middle of the Fc moiety. Only the N_{Fc} anions closest to the interface are included, with the number of Fc moieties N_{Fc}. The first peak for all anions and both fractions is at approximately 5 Å, corresponding to a contact between Fc and anion. Small differences in peak positions can be explained by anion sizes. This peak is higher for more hydrophobic anions (cf. ΔA_{hyd} in Table 1), except for $TFSI^-$, presumably due to its large size. For completeness, $TFSI^-$ is included in the figure but since the force field does not appear to be suited for the system, a detailed analysis is not provided.

In combination, Figures 3, 4 show an anion layering at the height of the Fc moieties, with anions packed between Fc moieties. This effect is strongest for the hydrophobic ClO_4^-, but even for the hydrophilic NO_3^-, some anions are nested between Fc moieties. Experimental setups often feature higher Fc fractions, χ_{Fc}, presumably hindering anions from moving into the space between Fc moieties. However, setups with smaller χ_{Fc} are not uncommon, and even for large χ_{Fc}, there can be domains with isolated Fc moieties.[9] Regardless, the results show that anions are in direct contact with Fc moieties, and this effect is stronger for more hydrophobic anions unless hindered by large anion sizes.

6. Conclusion

The results show that the redox potential of Fc-terminated monolayers is closely linked to the hydrophobicity of anion species in the electrolyte and hydrophobic anions build more pronounced layers at the Fc^+ cations. This is consistent with experiments and their discussions[7,8,10–12,30] as well as a computational work.[19] To form an anion layer at the oxidized monolayer, the anions must be removed from the bulk water. Thus, the free energy of hydration in the bulk contributes to the redox potential. Calculations of the energy of hydration at the interface could further illuminate the process. The hydrophobicity at the interface can differ substantially from bulk values and in fact the difference between the two values facilitates the oxidation. Hence, it would be instructive to compute the energy as a function of the distance from the interface based on cavity formation in water.[48–50] However, the interface between the monolayer and water poses new challenges for this approach because one needs to sample a large configuration space of Fc orientations. Furthermore, hydration energies of single anions as a function of distance from the interface would not replace the need for free energy calculations for the full anion layer, whereas this energy is included in the TI calculations in this work.

The presented computational approach combines a TI and the CCM to calculate the redox potential of Fc-terminated monolayer. This allows for a larger surface concentration of Fc moieties than in previous works[17,19] which is an important step toward full coverages often used in experiments.

In order to predict the shape of the peak in a cyclic voltammogram different approaches such as computational cyclic voltammetry[51,52] may be required. Here, Monte Carlo steps may help to find favorable configurations of mixed states with both Fc and Fc^+.

Appendix A: Theoretical Background

A.1. Thermodynamic Integration

Here we present a derivation for Equation 5. The difference in free energy at λ_k

$$A(\lambda_k+\delta\lambda)-A(\lambda_k) = -\beta^{-1}\ln\frac{\int \mathrm{d}^{3N}r\int \mathrm{d}^{3N}p\exp\left[-\beta\mathcal{H}_{\lambda_k+\delta\lambda}(r,p)\right]}{\int \mathrm{d}^{3N}r'\int \mathrm{d}^{3N}p'\exp\left[-\beta\mathcal{H}_{\lambda_k}(r',p')\right]}$$

$$= -\beta^{-1}\ln\int \mathrm{d}^{3N}r\int \mathrm{d}^{3N}p P_{\lambda_k}(r,p)$$

$$\times \exp\left(-\beta\left[\mathcal{H}_{\lambda_k+\delta\lambda}(r,p) - \mathcal{H}_{\lambda_k}(r,p)\right]\right)$$

$$= -\beta^{-1} \ln\left\langle \exp\left(-\beta\left[U_{\lambda_k+\delta\lambda}(r) - U_{\lambda_k}(r)\right]\right)\right\rangle_{\lambda_k} \quad \text{(A1)}$$

is expressed as an average over the ensemble using the probability density

$$P_\lambda(r,p) = \frac{1}{N!h^{3N}} \frac{\exp\left(-\beta\mathcal{H}_\lambda(r,p)\right)}{Q(\lambda)}. \quad \text{(A2)}$$

A.2. Constrained Charge Method

In the CCM, a Gaußian charge distribution

$$\chi_i(\mathbf{r}) = q_i\left(\frac{\eta_i^2}{\pi}\right)^{3/2} \exp\left[-\eta_i^2(\mathbf{r}-\mathbf{r}_i)^2\right] \quad \text{(A3)}$$

with the reciprocal width η is used to model the charges of electrode atoms. The Coulomb energy is calculated with an Ewald summation.[53] The electrode energy

$$U^{(\text{ele})}(\mathbf{q}) = \frac{1}{2}\mathbf{q}^\mathsf{T}\mathbf{A}\mathbf{q} + \mathbf{b}^\mathsf{T}\mathbf{q} \quad \text{(A4)}$$

is written as a function of $\mathbf{q}$, a vector of all electrode charges, and comprises the electrode-electrode interaction and the electrode-electrolyte interaction of the Coulomb energy.

Acknowledgements

The authors acknowledge funding by the Deutsche Forschungsgemeinschaft (DFG, German Research Foundation) – Projektnummer 192346071 – SFB 986, 390794421 – GRK 2462, and through the Cluster of Excellence EXC3120 BlueMat: Water-Driven Materials.

Open access funding enabled and organized by Projekt DEAL.

Conflict of Interest

The authors declare no conflict of interest.

Data Availability Statement

The data that support the findings of this study are available from the corresponding author upon reasonable request.

Keywords

free energy perturbation, redox reaction, self-assembled monolayer, solid-liquid interface

Received: May 6, 2025
Revised: July 11, 2025
Published online:

[1] Z. Zhang, L. Wen, L. Jiang, *Nat. Rev. Mater.* **2021**, *6*, 622.
[2] T. Juarez, J. Biener, J. Weissmüller, A. M. Hodge, *Adv. Eng. Mater.* **2017**, *19*, 1.
[3] G. Y. Gor, P. Huber, N. Bernstein, *Appl. Phys. Rev.* **2017**, *4*, 1.
[4] C. E. Chidsey, C. R. Bertozzi, T. M. Putvinski, A. M. Mujsce, *J. Am. Chem. Soc.* **1990**, *112*, 4301.
[5] S. E. Creager, G. K. Rowe, *Anal. Chim. Acta* **1991**, *246*, 233.
[6] G. K. Rowe, S. E. Creager, *Langmuir* **1991**, *7*, 2307.
[7] G. Valincius, G. Niaura, B. Kazakevičiene, Z. Talaikyte, M. Kažemekaite, E. Butkus, V. Razumas, *Langmuir* **2004**, *20*, 6631.
[8] X. Yao, J. Wang, F. Zhou, J. Wang, N. Tao, *J. Phys. Chem. B* **2004**, *108*, 7206.
[9] L. Y. S. Lee, T. C. Sutherland, S. Rucareanu, R. B. Lennox, *Langmuir* **2006**, *22*, 4438.
[10] L. L. Norman, A. Badia, *J. Phys. Chem. C* **2011**, *115*, 1985.
[11] A. V. Rudnev, U. Zhumaev, T. Utsunomiya, C. Fan, Y. Yokota, K. I. Fukui, T. Wandlowski, *Electrochim. Acta* **2013**, *107*, 33.
[12] R. A. Wong, Y. Yokota, M. Wakisaka, J. Inukai, Y. Kim, *Nat. Commun.* **2020**, *11*, 4194.
[13] Y. Yokota, Y. Mino, Y. Kanai, T. Utsunomiya, A. Imanishi, M. A. Wolak, R. Schlaf, K.-i. Fukui, *J. Phys. Chem. C* **2014**, *118*, 10936.
[14] W. Humphrey, A. Dalke, K. Schulten, *J. Mol. Graph.* **1996**, *14*, 33, arXiv: 1503.05249v1.
[15] F. C. Lima, A. Calzolari, M. J. Caldas, R. M. Iost, F. N. Crespilho, H. M. Petrilli, *J. Phys. Chem. C* **2014**, *118*, 23111.
[16] Y. Yokota, S. Akiyama, Y. Kaneda, A. Imanishi, K. Inagaki, Y. Morikawa, K.-i. Fukui, *J. Phys. Chem. C* **2016**, *120*, 8684.
[17] G. Filippini, F. Goujon, C. Bonal, P. Malfreyt, *J. Phys. Chem. B* **2010**, *114*, 12897.
[18] G. Filippini, Y. Israeli, F. Goujon, B. Limoges, C. Bonal, P. Malfreyt, *J. Phys. Chem. B* **2011**, *115*, 11678.
[19] G. Filippini, F. Goujon, C. Bonal, P. Malfreyt, *Soft Matter* **2011**, *7*, 8961.
[20] R. Marcus, N. Sutin, *Biochimica et Biophysica Acta (BBA) - Reviews on Bioenergetics* **1985**, *811*, 265.
[21] R. W. Zwanzig, *J. Chem. Phys.* **1954**, *22*, 1420.
[22] M. I. G. Nicholson, P. R. Bueno, G. T. Feliciano, *J. Phys. Chem. A* **2021**, *125*, 25.
[23] J. G. Kirkwood, *J. Chem. Phys.* **1935**, *3*, 300.
[24] M. Mezei, *J. Chem. Phys.* **1986**, *86*, 7084.
[25] L. J. Ahrens-Iwers, M. Janssen, S. R. Tee, R. H. Meißner, *Chin. J. Chem. Phys.* **2022**, *157*, 084801.
[26] J. I. Siepmann, M. Sprik, *J. Chem. Phys.* **1995**, *102*, 511.
[27] S. K. Reed, O. J. Lanning, P. A. Madden, *Chin. J. Chem. Phys.* **2007**, *126*, 084704.
[28] F. Schreiber, *Prog. Surf. Sci.* **2000**, *65*, 151.
[29] N. Nerngchamnong, D. Thompson, L. Cao, L. Yuan, L. Jiang, M. Roemer, C. A. Nijhuis, *J. Phys. Chem. C* **2015**, *119*, 21978.
[30] H. Ju, D. Leech, *Phys. Chem. Chem. Phys.* **1999**, *1*, 1549.
[31] W. L. Jorgensen, D. S. Maxwell, J. Tirado-Rives, *J. Am. Chem. Soc.* **1996**, *118*, 11225.
[32] G. Kaminski, E. M. Duffy, T. Matsui, W. L. Jorgensen, *J. Phys. Chem.* **1994**, *98*, 13077.
[33] J. N. Canongia Lopes, P. Cabral Do Couto, M. E. Minas Da Piedade, *J. Phys. Chem. A* **2006**, *110*, 13850.
[34] B. Rai, P. Sathish, C. P. Malhotra, Pradip, K. G. Ayappa, *Langmuir* **2004**, *20*, 3138.
[35] F. Goujon, C. Bonal, B. Limoges, P. Malfreyt, *Langmuir* **2009**, *25*, 9164.
[36] F. Goujon, C. Bonal, B. Limoges, P. Malfreyt, *J. Phys. Chem. B* **2010**, *114*, 6447.
[37] S. V. Sambasivarao, O. Acevedo, *J. Chem. Theory Comput.* **2009**, *5*, 1038.
[38] B. Doherty, X. Zhong, S. Gathiaka, B. Li, O. Acevedo, *J. Chem. Theory Comput.* **2017**, *13*, 6131.
[39] W. L. Jorgensen, J. Chandrasekhar, J. D. Madura, R. W. Impey, M. L. Klein, *J. Chem. Phys.* **1983**, *79*, 926.
[40] A. P. Thompson, H. M. Aktulga, R. Berger, D. S. Bolintineanu, W. M. Brown, P. S. Crozier, P. J. in 't Veld, A. Kohlmeyer, S. G. Moore, T. D.

Nguyen, R. Shan, M. J. Stevens, J. Tranchida, C. Trott, S. J. Plimpton, *Comput. Phys. Commun.* **2022**, *271*, 108171.
[41] github.com/robeme/lammps/tree/feature-fep, **2024**.
[42] E. R. Smith, *Proc. R. Soc. London A* **1981**, *375*, 475.
[43] I. C. Yeh, M. L. Berkowitz, *Chin. J. Chem. Phys.* **1999**, *111*, 3155.
[44] L. J. Ahrens-Iwers, R. H. Meißner, *Chin. J. Chem. Phys.* **2021**, *155*, 104104.
[45] S. Nosé, *J. Chem. Phys.* **1984**, *81*, 511.
[46] W. G. Hoover, *Phys. Rev. A* **1985**, *31*, 1695.
[47] A. I. Jewett, D. Stelter, J. Lambert, S. M. Saladi, O. M. Roscioni, M. Ricci, L. Autin, M. Maritan, S. M. Bashusqeh, T. Keyes, R. T. Dame, J. E. Shea, G. J. Jensen, D. S. Goodsell, *J. Mol. Biol.* **2021**, *433*, 166841.
[48] D. T. Limmer, A. P. Willard, P. A. Madden, D. Chandler, *Proc. Natl. Acad. Sci. USA* **2013**, *110*, 4200.
[49] A. Serva, M. Salanne, M. Havenith, S. Pezzotti, *Proc. Natl. Acad. Sci. USA* **2021**, *118*, 1.
[50] M. Bin Jassar, Q. Yao, F. Siro Brigiano, W. Chen, S. Pezzotti, *J. Phys. Chem. Lett.* **2024**, *15*, 11961.
[51] G. S. Karlberg, T. F. Jaramillo, E. Skúlason, J. Rossmeisl, T. Bligaard, J. K. Nørskov, *Phys. Rev. Lett.* **2007**, *99*, 1.
[52] N. Bergmann, N. G. Hörmann, K. Reuter, *J. Chem. Theory Comput.* **2023**, *19*, 8815.
[53] T. R. Gingrich, M. Wilson, *Chem. Phys. Lett.* **2010**, *500*, 178.